Development of a visible-light-responsive rutile rod by site-selective modification of iron(III) ion on {1 1 1} exposed crystal faces

著者	Murakami Naoya, Ono Asami, MisaNakamura, Tsubota Toshiki, Ohno Teruhisa
journal or publication title	Applied Catalysis B: Environmental
volume	97
number	1-2
page range	115-119
year	2010-06-09
URL	http://hdl.handle.net/10228/00006580

doi: info:doi/10.1016/j.apcatb.2010.03.030

Development of a visible-light-responsive rutile rod by site-selective modification of iron(III) ion on {1 1 1} exposed crystal faces

Naoya Murakami, Asami Ono, Misa Nakamura, Toshiki Tsubota and Teruhisa Ohno*

Department of Applied Chemistry, Faculty of Engineering, Kyushu Institute of Technology, 1-1 Sensuicho, Tobata, Kitakyushu 804-8550, Japan

Abstract

Trivalent iron(III) (Fe^{3+}) ions were site-selectively modified on {111} exposed crystal faces of shape-controlled rutile titanium(IV) oxide (TiO_2) by utilizing adsorption property of iron(III)/iron(II) (Fe^{3+}/Fe^{2+}) ion. The rutile TiO_2 with site-selective modification of Fe^{3+} ion showed high photocatalytic activity under visible-light irradiation as a result of separation of redox sites, i.e., oxidation and reduction proceed over Fe^{3+} ion modified on {111} faces and bare TiO_2 surface on {110} faces, respectively. Double-beam photoacoustic spectroscopic analyses suggest that the high activity of the TiO_2 with site-selective modification of Fe^{3+} ion is attributed to not an efficient electron injection from Fe^{3+} ion but an efficient reduction by injected electron on {110} faces.

* Corresponding author. FAX: +81-93-884-3318

E-mail address: tohno@che.kyutech.ac.jp (T. Ohno).

1. Introduction

Environmental purification with a utilization of self-cleaning effect on a semiconductor photocatalyst has attracted much attention [1,2]. Among various kinds of semiconductor photocatalyst, titanium(IV) oxide (TiO_2) is most suitable photocatalyst for an application of environmental purification in the view point of chemical stability, availability and no toxic properties. However, only fault of TiO_2 photocatalyst is inactive under visible-light irradiation because of its wide bandgap energy (3.0 eV for rutile and 3.2eV for anatase), i.e., ultraviolet (UV) light, the amount of which corresponds to only few percentage of total solar energy, is essential for photocatalytic reaction over TiO_2 photocatalyst.

So many intensive efforts to improve the visible-light responsibility of TiO_2 photocatalyst involving impurity doping have been made in the last few decades [3-8]. However, impurity doping sometimes increase defects in TiO_2, which also work as recombination center and result in decrease of photocatalytic activity [9,10]. Recently, some visible-light responsive TiO_2 photocatalyst were developed by modification of metal surface complex which works as a sensitizer for a visible light [11-15]. This method has large advantages in simple preparation method and no introduction of defects in TiO_2. In our previous study, the method was applied to titania nanotube, and metal ion was site-selectively modified outside/inside surface of titania nanotube for separation of photocatalytic redox sites [16]. Although its tubular structure enabled site-selective modification of metal ion, diffusion-controlled reaction was inevitable on the inside surface of TNT. Therefore, it is necessary for further improvement of photocatalytic activity under visible-light irradiation to modify metal ion site-selectively in the specific site on TiO_2 particles.

A utilization of shape-controlled particles with specific exposed crystal faces may be another plausible method for site-selective modification in specific site. It is well known that physical and chemical properties of semiconductor particles strongly depend on exposed crystal faces [17-19]. For example, certain chemical compounds work as shape-control reagent during nucleation process by preferential adsorption on specific crystal faces [20]. Therefore, site-selective modification of metal ion on shape-controlled nanocrystal may be possible by preferential adsorption properties

depending on crystal surface. Our studies suggest that redox reaction proceed preferentially on specific exposed crystal faces of TiO_2, i.e., reduction on {110} and oxidation on {111} for rutile, reduction on {011} and oxidation on {001} for anatase [21-23]. This kind of preferential reaction induces site-selective deposition of metal or metal oxide on the specific exposed crystal faces under photoexcitation [21-25].

In the present study, we modified iron(III) (Fe^{3+}) ion on shape-controlled rutile TiO_2 with specific exposed crystal faces. In our previous report, modification of Fe^{3+} ion on rutile TiO_2 largely improved photocatalytic reaction under visible-light irradiation by working as a sensitizer for visible light. Moreover, characteristic adsorption properties of Fe^{3+}/Fe^{2+} ion on TiO_2, which is strongly depended on valence states of iron ion, induced site-selective adsorption on the specific exposed crystal faces on the rutile TiO_2 particle.

2. Experimental

2.1. Sample preparation

2.1.1. Preparation of rutile rod

50 dm^3 of aqueous titanium(III) chloride solution (0.15 mol dm^{-3}) containing sodium chloride (5 mol dm^{-3}) in a Teflon bottle was stirred for 1 h, and then the bottle sealed with a stainless jacket was heated at 200 °C for 6 h in an oven. After the hydrothermal treatment, the residue in the Teflon bottle was washed with Milli-Q water several times until ionic conductivity was <10 μS cm^{-1}. The particles were dried under reduced pressure. In the present study, commercial rutile TiO_2 (TAYCA, MT-600B) with 27 m^2 g^{-1} of specific surface area was used as a reference sample.

2.1.2. Non-site-selective modification of Fe^{3+} ion on the entire surface

An aqueous suspension composed of samples and an aqueous solution of iron(III) nitrate ($Fe(NO_3)_3$) was stirred for 6 h under an aerated condition. After stirring, the supernatant and residue was separated by filtration, and the residue was washed with deionized water several times until the ionic conductivity of the supernatant was <10 μS cm^{-2} in order to remove NO_3^- ion, and

then the particles were dried under reduced pressure.

2.1.3. Site-selective modification of Fe^{3+} ions on specific exposed faces

An aqueous suspension composed of samples and an aqueous solution of $Fe(NO_3)_3$ with and without ethanol was stirred for 6 h under an aerated condition. The stirring was carried out under UV irradiation with a 500-W super-high-pressure mercury lamp (Ushio, SX-UI501UO), the light intensity of which was 1.0 mW cm^{-2}. The supernatant and residue was separated by filtration immediately after 6 h of the stirring. The residue was washed with deionized water several times until the ionic conductivity of the supernatant was <10 μS cm^{-1}, and then the particles were dried under reduced pressure.

2.2. Characterization

The crystal structures of the powders were confirmed by using an X-ray diffractometer (Rigaku, MiniFlex II) with Cu Kα radiation (λ = 1.5405 Å). The diffuse reflectance (DR) spectra were measured using a UV-VIS spectrophotometer (Shimadzu, UV-2500PC) equipped with an integrating sphere unit (Shimadzu, ISR-240A). The specific surface areas of the particles were determined with a surface area analyzer (Quantachrome, Nova 4200e) by using the Brunauer-Emmett-Teller equation. The morphology of prepared TiO_2 particles was observed by using transmission electron microscopy (TEM; Hitachi, H-9000NAR) and scanning electron microscopy (SEM; JEOL, JSM-6701FONO). The net amount of Fe^{3+} ions on the TiO_2 surface was estimated by analysis of filtrate with inductively coupled plasma optical emission spectroscopy (ICP-OES; Shimadzu, ICPS-8000). X-ray photoelectron spectra (XPS) of the TiO_2 particles were measured using a photoelectron spectrometer (JEOL, JPS90SX) with an Mg Kα source (1253.6 eV). The shift of binding energy was corrected using the C 1s level at 284.6 eV as an internal standard.

2.3. Photocatalytic decomposition of acetaldehyde

Photocatalytic activities of samples were evaluated by photocatalytic decomposition over

acetaldehyde. One hundred milligrams of powder, which has a complete extinction of the incident radiation, was spread on a glass dish, and the glass dish was placed in a 125 cm^3 Tedlar bag (AS ONE Co. Ltd.). Five hundred parts per million of gaseous acetaldehyde was injected into the Tedlar bag, and photoirradiation was performed at room temperature after the acetaldehyde had reached adsorption equilibrium. The gaseous composition in the Tedlar bag was 79% of N_2, 21% of O_2, < 0.1 ppm of CO_2 and 500 ppm of acetaldehyde, and relative humidity was ca. 30%. A light emitting diode (LED; Lumileds, Luxeon LXHL-NRR8), which emitted light at a wavelength of ca. 455 nm with an intensity of 1.0 mW cm^{-2}, was used for visible light irradiation. The emission spectrum of the LED is shown in figure 1. The concentrations of acetaldehyde and carbon dioxide (CO_2) were estimated by gas chromatography (Shimadzu, GC-8A, FID detector) with a PEG-20 M 20% Celite 545 packed glass column and gas chromatography (Shimadzu, GC-9A, FID detector) with a TCP 20% Uniport R packed column and a methanizer (GL Sciences, MT-221), respectively.

2.4. Double-beam photoacoustic spectroscopic measurement

A gas-exchangeable photoacoustic (PA) cell equipped with two valves for gas flow was used, and a TiO_2 sample was placed in the cell. The atmosphere was controlled by a flow of nitrogen containing ethanol vapor (N_2 + EtOH) or artificial air containing ethanol vapor (air + EtOH), and the measurements were conducted after shutting off the valves, i.e., in a closed system at room temperature. A LED emitting light at ca. 625 nm (Lumileds, Luxeon LXHL-ND98) was used as a probe light, and the output intensity was modulated by a digital function generator (NF, DF1905) at 80 Hz. In addition to the modulated light, a blue-LED (Lumileds, Luxeon LXHL-NB98, emitting light at ca. 470 nm, 8.1 mW cm^{-2}) was also used as simultaneous continuous irradiation for photoexcitation. The PA signal acquired by a condenser microphone buried in the cell was amplified and monitored by a digital lock-in amplifier (NF, LI5640). Detailed setups of double-beam photoacoustic (DB-PA) spectroscopic measurements have been reported previously [26].

3. Results and discussion

3.1. Physical and chemical properties of bare and Fe^{3+}-modified TiO_2 samples

The crystal structure of sample prepared by hydrothermal treatment of titanium(III) chloride solution in the presence of sodium chloride was attributed to rutile TiO_2 without other crystal phases from XRD pattern. Moreover, SEM, TEM and electron diffraction analyses indicate that prepared TiO_2 has rod shape with {110} and {111} exposed crystal faces. The specific surface area of the bare rutile rod was 34 m^2 g^{-1}. These results coincident with the reported studies [23,27,28].

Table 1 shows summary of Fe^{3+}-modified samples prepared by three kinds of Fe^{3+}-modification method. Valence state of iron ion on TiO_2 particles was confirmed to be trivalent state by XPS analyses. UV irradiation during Fe^{3+} modification decreased net amount of Fe^{3+} ion modified on the TiO_2 surface while almost of Fe^{3+} ion was modified on the TiO_2 surface in dark. It is reported that Fe^{2+} ion hardly adsorb on TiO_2 surface compared to Fe^{3+} ion [29]. Therefore, it is thought that Fe^{2+} ion was produced as a result of reduction of Fe^{3+} ion by photoexcited electron in TiO_2 and then produced Fe^{2+} ion desorbed from TiO_2 surface. Addition of ethanol decreased net amount of modified Fe^{3+} ion because reduction of Fe^{3+} ion was accelerated due to an electron accumulation in TiO_2, which was induced by efficient hole consumption.

Our previous study suggested that reduction and oxidation on the rutile rod proceed predominantly on {110} and {111} exposed crystal faces, respectively [23]. Therefore, Fe^{3+} ions mainly are expected to adsorb on {111} faces under UV irradiation because Fe^{3+} ion on {110} faces desorbs due to reduction of Fe^{3+} to Fe^{2+} (Scheme 1). Produced Fe^{2+} ion is thought to be recovered to Fe^{3+} ion as a result of reoxidation by oxygen and/or positive holes on {111} faces [30]. Actually, further decrease of net amount of modified Fe^{3+} ion was observed in same modification method under deaerated condition.

Modification of Fe^{3+} ion induced color change form white to pale yellow as reported in previous study [15]. Figure 1 show UV-vis spectra of bare and Fe^{3+}-modified TiO_2. In the wavelength region between 400-500 nm of DR spectra, an upward shift of photoabsorption was observed.

Photoabsorption was increased with an increase of net amount of Fe^{3+} ion in the TiO_2 prepared by same modification method. However, increase of photoabsorption disagreed with net amount of modified Fe^{3+} ion among D-01, P-01 and PE-01. This indicate that not only amount of Fe^{3+} ion but also modification method have an influence in photoabsorption of Fe^{3+}.

3.2. Photocatalytic activity for decomposition of acetaldehyde under visible light irradiation

Figure 2 shows time course of CO_2 evolution for decomposition of acetaldehyde under visible-light irradiation. Photocatalytic activity of Fe^{3+}-modified TiO_2 was higher than bare TiO_2. This indicate that Fe^{3+} ion modified on TiO_2 induce photocatalytic reaction under visible-light irradiation as follows [15]; (1) photoexcited Fe^{3+} ions injected electrons into TiO_2 and became an oxidized state of Fe^{3+} (Fe^{4+}), (2) injected electrons migrated in the bulk and reduced oxygen species on TiO_2 surface and (3) the oxidized state of Fe^{3+} ions (Fe^{4+}) oxidized acetaldehyde and go back to the initial state of metal ions (Fe^{3+}). PE-01 and P-01 showed higher photocatalytic activity than nitrogen-doped TiO_2 (N-TiO_2; Sumitomo Chemical Co.), which is well-known as a conventional visible-light responsive TiO_2. Moreover, photocatalytic activity of Fe^{3+}-modified TiO_2 showed dependence on its preparation method (PE-01 > P-01 > D-01). There are three plausible reasons for difference of photocatalytic activity; (1) net amount of Fe^{3+} modified on TiO_2, (2) structure of Fe^{3+} species depending on modification condition and (3) site selectivity of Fe^{3+} modification. In order to make clear it, following experiments were carried out.

Figure 3 shows dependence of net amount of Fe^{3+} ion modified on photocatalytic activity (CO_2 evolution at 240 min of photoirradiation). Photocatalytic activity was increased by small amount of Fe^{3+} modification because of increase of visible-light photoabsorption. On the other hand, an excess amount of Fe^{3+} modification decreased photocatalytic activity presumably due to decrease of reduction sites by coverage of TiO_2 surface and/or formation of inactive aggregated Fe^{3+} species. Therefore, increase of photocatalytic activity of Fe^{3+}-modified rutile nanorod prepared by UV irradiation might be attributable to the removal of an excess amount of Fe^{3+} because UV irradiation decreased net amount of Fe^{3+} ion as indicated in table 1. However, the hypothesis is denied by a

different dependence of photocatalytic activity on net amount of Fe^{3+} ion of non-site-selective Fe^{3+} modified rutile nanorod as indicated in figure 3. Thus, high photocatalytic activity of Fe^{3+}-modified rutile nanorod prepared by UV-irradiation was not attributed to removal of excess amount of Fe^{3+} ion.

Same modification method was applied to commercial rutile TiO_2, which has spherical shape without specific exposed crystal faces. Therefore, UV irradiation during Fe^{3+} modification is thought to induce no site-selective modification on the particle because redox reaction proceeds in the neighboring sites without being separated. Figure 4 shows time course of CO_2 evolution for decomposition of acetaldehyde over Fe^{3+}-modified commercial rutile under visible-light irradiation. These two samples were prepared by different kind of modification method, but same net amount of Fe^{3+} ion was modified between these samples by adjusting initial amount of Fe^{3+}. A large difference of photocatalytic reaction was not observed, regardless of the presence or absence of UV irradiation during Fe^{3+} modification. This indicate that the UV irradiation induced formation of same Fe^{3+} species for photocatalytic reaction as that prepared in dark. Therefore, the reason for high activity of P- and PE-samples is that UV irradiation during Fe^{3+} modification induces site-selective modification of Fe^{3+} ion.

An excess amount of Fe^{3+} modification decreased photocatalytic activity even for P-samples because saturation limit of Fe^{3+} modification on {111} faces deteriorate site-selectively of Fe^{3+} modification, resulting in modification of Fe^{3+} ion on {110} faces. Moreover, D-samples show lower photocatalytic activity than DMT (Fig. 2 and Fig. 4). This indicate that modification on {110} faces decrease photocatalytic activity because an efficient reduction on {110} faces was retarded due to coverage of Fe^{3+} ion.

3.3. PA spectroscopic detection of electron behavior under visible-light irradiation

Behavior of injected electron in TiO_2 was observed by DB-PAS [26]. Figure 5 shows time-course curve of PA intensity for D-01, P-01, PE-01 and bare TiO_2 under visible-light irradiation in the presence of N_2 + EtOH. PA intensity increased with visible-light irradiation

because Ti^{4+} was reduced to Ti^{3+} by injected electrons from photoexcited Fe^{3+} ion. Thus, increase of PA intensity is attributed to amount of injected electrons. The saturation limit of PA intensity showed no dependence on Fe^{3+}-modification method. This is reasonable results because photoabsorption of these samples was not so different from each other. This indicate that the main factor of high photocatalytic activity was not oxidation on oxidized Fe^{3+} (Fe^{4+}) generated by electron injection from Fe^{3+} ion into TiO_2. Another plausible factor may be efficiency of reduction on rutile TiO_2 nanorod modified with Fe^{3+} by injected electron.

DB-PA measurements in the presence of oxygen were also carried out in order to estimate efficiency of reduction by injected electron. Figure 6 shows time-course curve of PA intensity for D-01, P-01, PE-01 and bare TiO_2 under visible-light irradiation in the presence of air + EtOH. PA intensity attributed to Ti^{3+} formation was largely decreased because an electron accumulation was retarded due to electron consumption by oxygen species on TiO_2 surface. Steady-state value of PA intensity showed dependence on modification method (D-01 > P-01 > PE-01), and site selectivity of Fe^{3+} modification induced smaller PA intensity. This suggests that reduction efficiently proceed on surface of P-01 and PE-01 than that of D-01 because an efficient reduction of oxygen on {110} faces proceeded without retardation by coverage of Fe^{3+} ion. The injected electron in the rutile nanorod is thought to be prevented from being trapped by oxidized Fe^{3+} (Fe^{4+}) because the injected electrons should be efficiently consumed on {111} faces.

4. Conclusion

UV irradiation during Fe^{3+}-modification on shape-controlled rutile TiO_2 induced high photocatalytic activity under visible-light irradiation because Fe^{3+} ion was site-selectively modified on {111} exposed crystal faces and redox reactions were spatially separated. On the other hand, photocatalytic activity of non-site-selectively modified TiO_2 showed low activity. DB-PA analyses indicate that photocatalytic activity was determined by not efficiency of electron injection but efficiency of reduction by injected electron. The efficiency of reduction was influenced by site-selectivity of Fe^{3+}-modification on {111} faces because Fe^{3+} ion on {110} faces retard an

efficient reduction on bare TiO_2 surface.

Acknowledgements

This work was supported by a grant of Knowledge Cluster Initiative implemented by the Ministry of Education, Culture, Sports, Science and Technology (MEXT) and the New Energy and Industrial Technology Development Organization (NEDO).

Table 1. Fe^{3+}-modified TiO_2 prepared by different kinds of method and samples.

Scheme 1. Site selective modification on the shape controlled rutile rod with {110} and {111} exposed crystal faces.

Figure 1. UV-vis spectra of (a) D-01, (b) P-01, (c) PE-01, (d) bare, and (e) D-032 and emission spectrum of LED used for photocatalytic evaluation.

Figure 2. Time courses of CO_2 evolution of acetaldehyde decomposition over (a) D-01, (b) P-01, (c) PE-01, (d) bare, and (e) N-TiO_2 under visible-light irradiation.

Figure 3. CO_2 evolution at 240 min of photoirradiation for photocatalytic decomposition over (a) D-samples, (b) P-samples, and (c) PE-01 as a function of net amount of Fe^{3+} ion.

Figure 4. Time courses of CO_2 evolution of acetaldehyde decomposition over (a) DMT and (b) PEMT under visible-light irradiation.

Figure 5. Time-course curves of PA signals of (a) D-01, (b) P-01, (c) PE-01, and (d) bare under visible light irradiation in the presence of N_2 + EtOH.

Figure 6. Time-course curves of PA signals of (a) D-01, (b) P-01, (c) PE-01, and (d) bare under visible light irradiation in the presence of air + EtOH.

Figure 6. Time-course curves of PA signals with 50 points smoothing of (a) D-01, (b) P-01, (c) PE-01, and (d) bare under visible light irradiation in the presence of air + EtOH.

References

[1] A. Fujishima, T. N. Rao, D. A. Tryk, J. Photochem. Photobiol. C: Photochem. Reviews 1 (2000) 79.

[2] M. R. Hoffmann, S. T. Martin, W. Choi and D. W. Bahnemann, Chem. Rev. 95 (1995) 69-96.

[3] S. Sato, Chem. Phys. Lett. 123 (1986) 126.

[4] R. Asahi, T. Morikawa, T. Ohwaki, K. Aoki, Y. Taga, Science 293 (2001) 269.

[5] T. Umebayashi, T. Yamaki, H. Itoh, K. Asai, Appl. Phys. Lett. 81 (2002) 454.

[6] T. Ohno, M. Akiyoshi, T. Umebayashi, K. Asai, T. Mitsui, M. Matsumura, Appl. Catal. A: Gen. 265 (2004) 115.

[7] T. Ohno, T. Tsubota, K.Nishijima, Z. Miyamoto, Chem. Lett. 33 (2004) 750.

[8] H. Irie, Y. Watanabe, K. Hashimoto, Chem. Lett. 32 (2003) 772.

[9] N. Serpone, D. Lawless, L angmuir 10 (1994) 643.

[10] S. Ikeda, N. Sugiyama, B. Pal, G. Marci, L. Palmisano, H. Noguchi, K. Uosakid, B. Ohtani, Phys. Chem. Chem. Phys. 3 (2001) 267.

[11] H. Kisch, L. Zang, C. Lange, W. F. Maier, C. Antonius, D. Meissner, Angew. Chem. Int. Ed. 37 (1998) 3034.

[12] L. Zang, C. Lange, I. Abraham, S. Storck, W. F. Maier, H. Kisch, J. Phys. Chem. B 102 (1998) 10765.

[13] L. Zang, W. Macyk, C. Lange, W. F. Maier, C. Antonius, D. Meissner, H. Kisch, Chem. Eur. J. 6 (2000) 379.

[14] W. Macyk, H. Kisch, Chem. Eur. J. 7 (2001) 1862.

[15] N. Murakami, T. Chiyoya, T. Tsubota, T. Ohno, Appl. Catal. A: Gen. 348 (2008) 148.

[16] N. Murakami, Y. Fujisawa, T. Tsubota, T. Ohno, Appl. Catal. B: Environ. 92 (2009) 56.

[17] P. A. Morris Hotsenpiller, J. D. Bolt, W. E. Farneth, J. B. Lowekamp, G.. S. Rohrer, J. Phys. Chem. B 102 (1998) 3216.

[18] J. B. Lowekamp, G. S. Rohrer, P. A. Morris Hotsenpiller, J. D. Bolt, W. E. Farneth, J. Phys. Chem. B 102 (1998) 7323.

[19] A. Imanishi, H. Suzuki, K. Murakoshi, Y. Nakato, J. Phys. Chem. B 110 (2006) 21050.

[20] C. G. Read, E. M. P. Steinmiller, K. Choi, J. Am. Chem. Soc. 131 (2009) 12040.

[21] T. Ohno, K. Sarukawa and M. Matsumura, New. J. Chem. 26 (2002) 1167.

[22] E. Bae, N. Murakami, T. Ohno, J. Molec. Catal. A: Chem. 300 (2009) 72.

[23] N. Murakami, Y. Kurihara, T. Tsubota, T. Ohno, J. Phys. Chem. C 113 (2009) 3062.

[24] H. Kato, K. Asakura, A. Kudo, J. Am. Chem. Soc. 125 (2003) 3082.

[25] Y. Matsumoto, S. Ida, T. Inoue, J. Phys. Chem. C 112 (2008) 11614.

[26] N. Murakami, O. O. P. Mahaney, R. Abe, T. Torimoto, B. Ohtani, J. Phys. Chem. C 111 (2007) 11927-11935.

[27] E. Hosono, S. Fujihara, K. Kakiuchi, K. Imai, J. Am. Chem. Soc. 126 (2004) 7790.

[28] K. Kakiuchi, E. Hosono, H. Imai, T. Kimura, S. Fujihara, J. Cryst. Growth 293 (2006) 541.

[29] T. Ohno, D. Haga, K. Fujihara, K. Kaizaki, M. Matsumura, J. Phys. Chem. B 101 (1997) 6415.

[30] W. Choi, A. Termin, M. R. Hoffmann, J. Phys. Chem. B 98 (1994) 13669.

Table 1. Fe^{3+}-modified TiO_2 prepared by different kinds of method and samples.

Name	Sample	Fe^{3+}(init) / wt%	Fe^{3+}(net) / wt%	preparation condition
D-004	rutile rod	0.04	0.04	dark
P-004	rutile rod	0.04	0.04	photo
D-01	rutile rod	0.10	0.10	dark
P-01	rutile rod	0.10	0.09	photo
PE-01	rutile rod	0.10	0.04	photo + EtOH
D-032	rutile rod	0.32	0.32	dark
P-032	rutile rod	0.32	0.22	photo
DMT	MT-600B	0.05	0.05	dark
PEMT	MT-600B	0.10	0.05	photo + EtOH

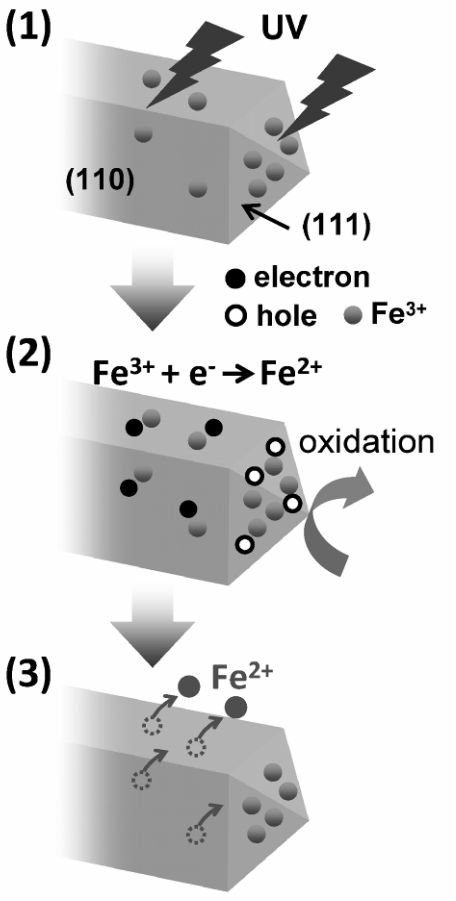

Scheme 1. Site selective modification on the shape controlled rutile rod with {110} and {111} exposed crystal faces.

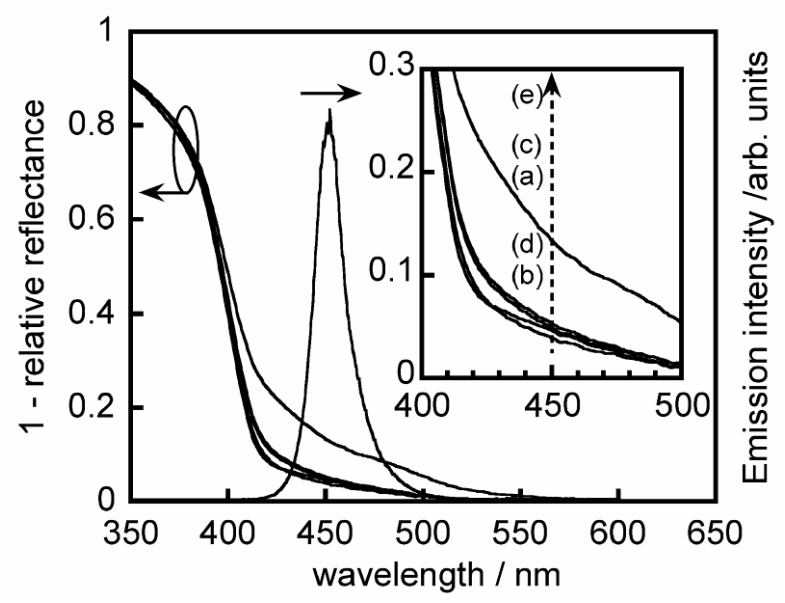

Figure 1. UV-vis spectra of (a) D-01, (b) P-01, (c) PE-01, (d) bare, and (e) D-032 and emission spectrum of LED used for photocatalytic evaluation.

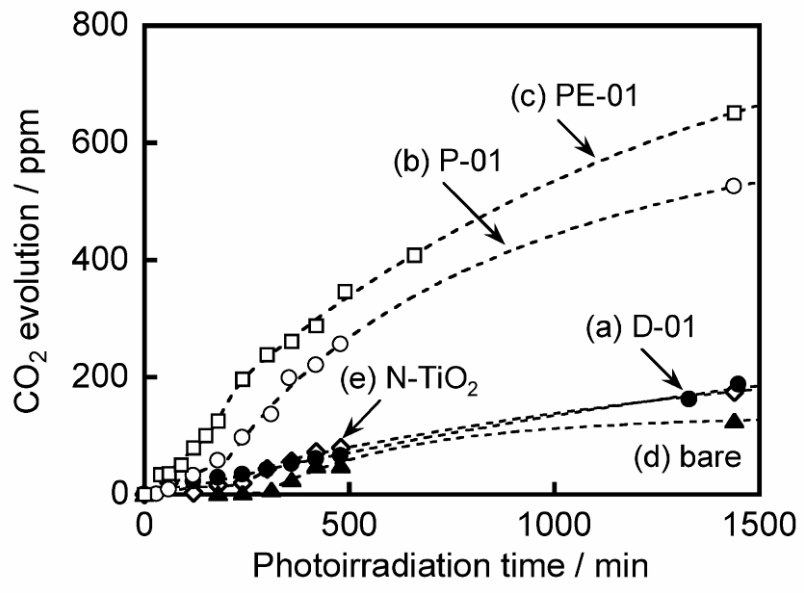

Figure 2. Time courses of CO_2 evolution of acetaldehyde decomposition over (a) D-01, (b) P-01, (c) PE-01, (d) bare, and (e) N-TiO_2 under visible-light irradiation.

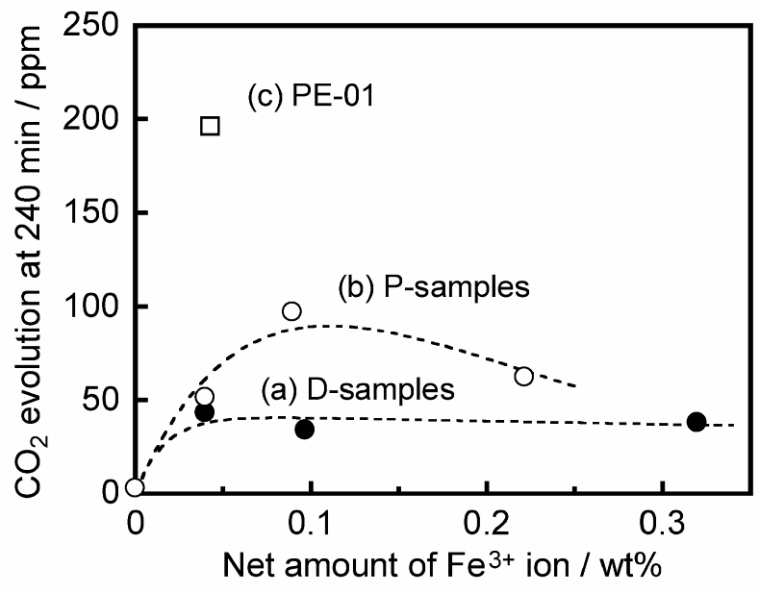

Figure 3. CO_2 evolution at 240 min of photoirradiation for photocatalytic decomposition over (a) D-samples, (b) P-samples, (c) PE-01 as a function of net amount of Fe^{3+} ion.

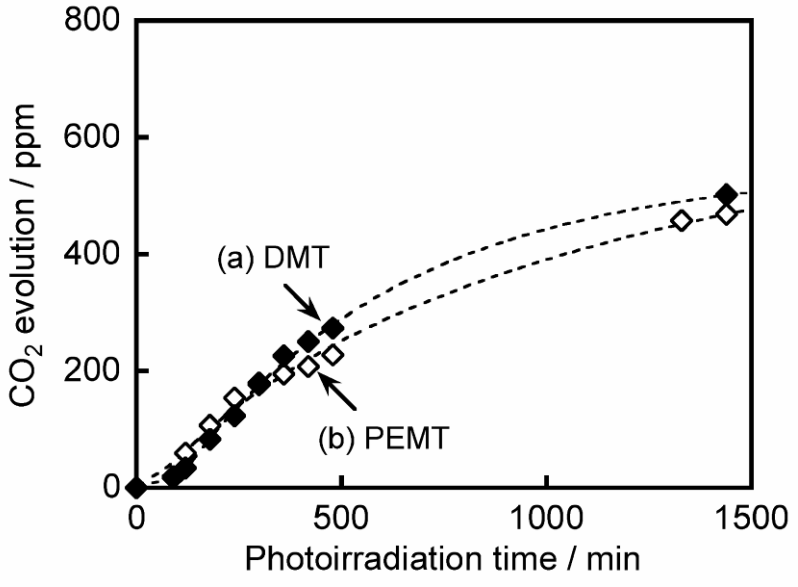

Figure 4. Time courses of CO_2 evolution of acetaldehyde decomposition over (a) DMT and (b) PEMT under visible-light irradiation.

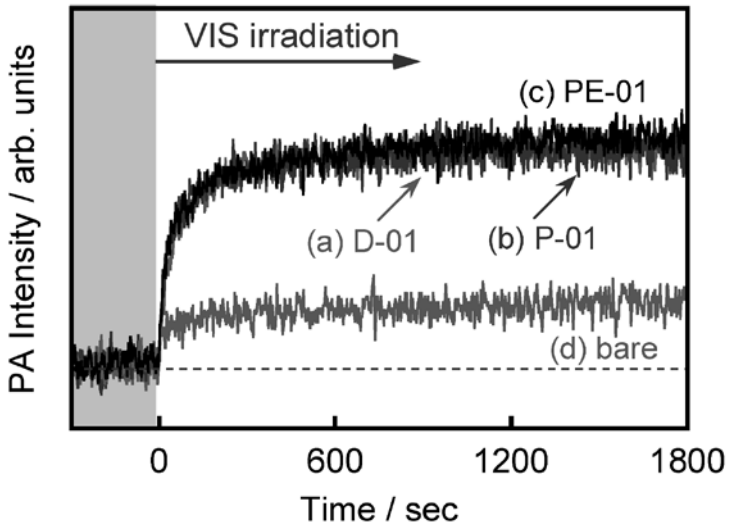

Figure 5. Time-course curves of PA signals of (a) D-01, (b) P-01, (c) PE-01, (d) bare under visible light irradiation in the presence of N_2 + EtOH.

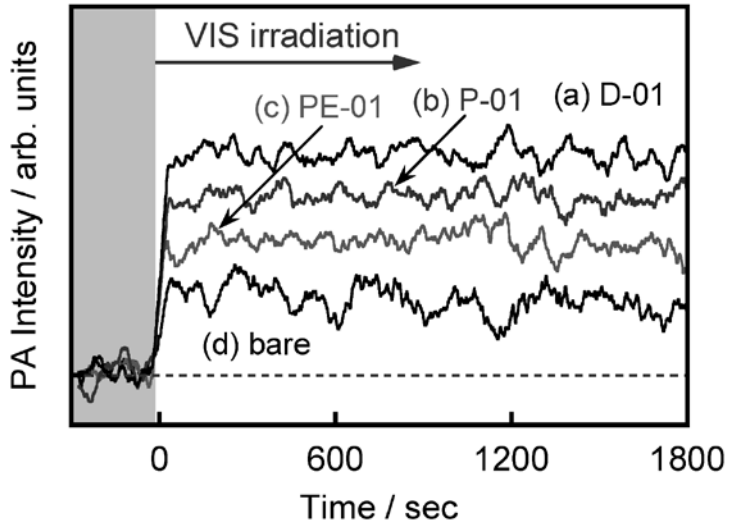

Figure 6. Time-course curves of PA signals with 50 points smoothing of (a) D-01, (b) P-01, (c) PE-01, (d) bare under visible light irradiation in the presence of air + EtOH.